ELSEVIER

Contents lists available at ScienceDirect

Inorganica Chimica Acta

journal homepage: www.elsevier.com/locate/ica



Research paper

An overly anionic metal coordination environment eliminates the T_1 -weighted response of quinol-containing MRI contrast agent sensors to H_2O_2



Tessa E. Hutchinson^a, Adam Bashir^a, Meng Yu^a, Ronald J. Beyers^b, Christian R. Goldsmith^{a,*}

ARTICLE INFO

Keywords:
Ligand design
Manganese
Magnetic resonance imaging
Sensors

ABSTRACT

A previously reported quinol- and Mn(II)-containing MRI contrast agent sensor for H_2O_2 has the drawback of releasing the metal ion upon oxidation of the organic ligand. The release of potentially neurotoxic Mn(II) limits the sensor's *in vivo* applicability. We prepared N_iN' -bis(2,5-dihydroxybenzyl)ethanediamine- N_iN' -diacetic acid (H_6 qc1) as a substitute ligand that could potentially remain bound to the metal ion after oxidation of the quinol portions to more weakly metal-binding *para*-quinones. The carboxylic acid groups deprotonate at ambient pH, providing a more anionic coordination environment that stabilizes its Mn(II) complex in water. Although the more anionic coordination sphere doesn't introduce air sensitivity, it does render the metal center more susceptible to oxidation by hydrogen peroxide, as evidenced by electron paramagnetic resonance. The oxidation of the metal to less paramagnetic Mn(III) is proposed to lower the r_1 enough to completely counter any increase in T_1 -weighted relaxivity that would result from improved aquation.

1. Introduction

The over-production of reactive oxygen species (ROS) has been associated with a wide range of health disorders, including several cardiovascular and neurological diseases [1–5]. The roles of ROS in these pathologies, however, have not been fully clarified. Being able to identify when and where ROS concentrations spike during disease progression could provide more effective means to both diagnose and treat these conditions. Spatiotemporal patterns of oxidative stress in the brain could, for instance, help to differentiate neurological conditions that give rise to similar clinically observable symptoms. In order to identify these and similar patterns, one needs a redox-active sensor that can reliably function *in vivo*. Probes that alter how tissues and organs appear when visualized by magnetic resonance imaging (MRI) are attractive in that this spectroscopic technique allows for non-invasive imaging.

Our laboratory has previously reported a series of redox-responsive contrast agents for MRI [6–8]. Our general strategy has been to complex a redox-active organic ligand to a Mn(II) ion. The high paramagnetism of high-spin Mn(II) (S=5/2) results in a high T_I -weighted relaxivity (r_I). The redox activity of manganese allows it to catalyze the oxidation of the organic component by a ROS. Our more recent work has focused on using polydentate ligands with quinols as the redox-active moieties [7,8]. Transition metal ion-catalyzed oxidation by H_2O_2 converts these

to *para*-quinones (Scheme 1), which are more readily displaced by water molecules. The greater aquation increases r_1 , improving MRI contrast, and a ligand with two quinols, H_4 qp2 (Scheme 2), provides a larger response [8].

The disadvantage of this strategy is that the oxidized ligand necessarily has a weaker binding affinity for Mn(II). Indeed, the reaction between $\rm H_2O_2$ and [Mn($\rm H_4qp2$)Br₂] likely releases a substantial amount of Mn(II), based on the relatively low stability of the pre-oxidized complex and the 2.8 aquation number (q) measured for the oxidized mixture [8]. The measured q is likely elevated by the presence of [Mn($\rm H_2O)_6$]²⁺ (q=6), but the partial oxidation of the quinols prevented us from more definitively assessing the stabilities of the oxidized products. Approximately 70% of the quinols are oxidized with excess $\rm H_2O_2$; this results in a mixture of Mn(II) complexes with unreacted $\rm H_4qp2$, a partially oxidized ligand with only one para-quinone ($\rm H_2qp2$), and the fully oxidized ligand with two para-quinones ($\rm qp2$). The loss of Mn(II) from the probe is problematic for $in\ vivo$ applications since free Mn(II) is known to be toxic [9].

In the current work, we attempt to eliminate oxidation-triggered release of Mn(II) by substituting carboxylate groups for the pyridines in H_4 qp2. Although such a substitution could be expected to lower the thermodynamic barrier for the oxidation of Mn(II) to Mn(III), Caravan's group had recently used phenol- and carboxylate-containing ligands to produce Mn(II) complexes that are sufficiently stable to air to use as

E-mail address: crgoldsmith@auburn.edu (C.R. Goldsmith).

^a Department of Chemistry and Biochemistry, Auburn University, Auburn, AL 36849, USA

^b Auburn University Magnetic Resonance Imaging Research Center, Auburn, AL 36849, USA

^{*} Corresponding author.

Scheme 1. Note that this graphic originally appeared in Ref. [8].

$$H_2$$
qp1 H_4 qp2 H_6 qc1 H

Scheme 2. Polydentate ligands discussed in this manuscript.

MRI contrast agents [10–12]. Further, the resulting ligand would have a strong resemblance to N,N'-bis(2-hydroxybenzyl)ethylenediamine-N,N'-diacetic acid (HBED, Scheme 2), which was synthesized and characterized by Martell and co-workers and forms a stable complex with Mn(II) [13,14]. Additionally, we have observed that a sufficiently redox-active ligand can direct redox chemistry away from the metal ion by serving as a sacrificial oxidant or reductant [15].

We synthesized N,N'-bis(2,5-dihydroxybenzyl)ethanediamine-N,N'-diacetic acid (H₆qc1, Scheme 2) as a new hexadentate ligand. This molecule retains the two quinols of H₄qp2 that are essential to the large H₂O₂ response of its Mn(II) complex but replaces the pyridines with carboxylic acids, which readily deprotonate to carboxylate anions above pH 5.0. The installation of the carboxylic acids is anticipated to improve the binding affinity of the ligand by providing a more anionic coordination environment for cationic metal ions at ambient pH. The ligand is otherwise similar to H₄qp2; this enables us to focus on determining how ligand charge impacts the stability of the sensor and its response to H₂O₂.

2. Experimental section

2.1. Materials

All chemicals were purchased from Sigma-Aldrich and used as received, unless noted otherwise. Diethyl ether (ether), ethyl acetate (EtOAc), methanol (MeOH), dichloromethane (CH_2Cl_2), and ethanol (EtOH) were bought from VWR. 1,2-Ethylenediamine was purchased from Fluka. All deuterated solvents were bought from Cambridge Isotopes and used as received.

2.2. Instrumentation

¹H and ¹³C NMR spectra were recorded on either a 400 MHz or 600 MHz AV Bruker NMR spectrometer. IR spectra were collected with a Nicolet iS-50 spectrometer. Electron paramagnetic resonance (EPR) spectra were collected on a Bruker EMX-6/1 X-band EPR spectrometer operated in the perpendicular mode and analyzed with the program EasySpin. All EPR samples were run as frozen solutions in quartz tubes. High-resolution mass spectrometry (HR-MS) data were obtained at the Mass Spectrometry Center at Auburn University on a Bruker microflex LT MALDI-TOF mass spectrometer via direct probe analysis operated in the positive ion mode.

2.3. Magnetic resonance imaging (MRI)

All MRI data were collected at the Auburn University MRI Research

Center on a Siemens Verio open-bore 3-T MRI clinical scanner; a 15channel knee coil was used to simultaneously image 12-15 samples. The imaging procedure was identical to those used for similar studies from our laboratory [6-8,16]. An inversion recovery (IR) sequence was used that featured a non-selective adiabatic inversion pulse followed by a slice-selective gradient recalled echo (GRE) readout after a delay period corresponding to the inversion time (TI) [17,18]. The GRE was a saturation readout, such that only one line of k-space was acquired per repetition time (TR), in order to maximize both signal strength and the accuracy of the T_1 estimates. The specific imaging parameters were as follows: TR was set to 4s, TI was varied from 4.8 to 2500 ms over 37 steps, the echo time (TE) was set to 3.6 ms, the flip angle equaled 90°, averages = 1, slice thickness = 5 mm, field of view = 140×140 mm, matrix = 128×128 , resulting in a pixel size of $1.1 \times 1.1 \times 5.0$ mm. All samples were run in aqueous solutions buffered to pH 7.0 and kept at 22 $^{\circ}\text{C}$. The manganese content was systematically varied from 0.10 to $1.00\,\mathrm{mM}$. The inverses of the T_1 values were plotted versus the concentration of Mn(II) to obtain r_1 values.

2.4. MRI data analysis

Image analysis was performed using custom Matlab programs (Mathworks, Natick, MA). The initial TI = 4.8 ms image was used as a baseline to determine circular region of interest (ROI) boundaries for each sample; from these, the mean pixel magnitudes for each ROI were calculated. For each of the 36 subsequent TI images, the same ROI boundaries were applied, and the mean pixel magnitude calculations were repeated. This gave consistent ROI spatial definitions and a corresponding time course of magnitudes for each of the samples over all the TI time points. Each sample's complex phase was used to correct the magnitude polarity to produce a complete exponential T_1 inversion recovery curve. The Nelder-Mead simplex algorithm [19] was applied to each sample's exponential curve to estimate its corresponding T_1 value.

2.5. Synthesis

2,5-Bis(tert-butyldimethylsiloxy)benzaldehyde (1)

This compound was prepared through a previously reported procedure [20]. 2,5-Dihydroxybenzaldehyde (700 mg, 5.07 mmol) and imidazole (1.04 g, 15.2 mmol) were dissolved in 10 mL of anhydrous N,N-dimethylformamide under a N_2 atmosphere. The resultant solution was then cooled to 0 °C using an ice bath. tert-Butyldimethylsilyl chloride (1.90 g, 12.6 mmol) was added, and the reaction mixture stirred and warmed to room temperature (RT) over the next 16 h. 100 mL of water were then added to quench the reaction, and the crude

product was extracted with three 50 mL portions of EtOAc. The organic layers were combined, washed with three 100 mL aliquots of water, and dried over sodium sulfate. After the EtOAc was removed by rotavaporation, the product was purified by column chromatography using 50:1 hexanes/EtOAc as the eluent ($R_f = 0.2$) to yield 1.60 g of the product as a yellow oil (85% yield). ¹H NMR (400 MHz, CDCl₃, 293 K): $\delta\,10.39~(\text{s},\,1\text{H}),\,7.24~(\text{m},\,1\text{H}),\,6.97~(\text{m},\,1\text{H}),\,6.76~(\text{m},\,1\text{H}),\,1.02~(\text{s},\,9\text{H}),$ 0.98 (s, 9H), 0.25 (s, 6H), 0.19 (s, 6H). ¹³C NMR (100 MHz, CDCl₃, 293 K): 189.9, 153.4, 149.8, 127.9, 127.4, 121.2, 117.7, 25.7, 25.6, 18.3, 18.1, -4.4, -4.5. MS (ESI): Calcd for MH⁺, 367.2125; Found, 367.1879. IR (cm⁻¹): 2955.36 (m), 2930.04 (m), 2886.00 (w), 2857.88 (m), 1686.29 (m), 1608.23 (w), 1485.10 (s), 1419.96 (m), 1387.18 (m), 1362.25 (w), 1300.30 (w), 1253.61 (s), 1209.72 (s), 1150.68 (s), 1006.29 (w), 983.85 (m), 909.32 (s), 836.98 (s), 821.89 (s), 805.21 (s), 777.97 (s), 732.67 (w), 684.67 (m), 668.07 (w), 640.88 (w), 611.26 (w), 581.31 (w), 537.82 (w), 449.69 (w).

N,N'-Bis[2,5-bis(tert-butyldimethylsiloxy)benzyl]-1,2-ethanediamine (2)

2,5-Bis(tert-butyldimethylsiloxy)benzaldehyde (1.10 g, 3.00 mmol) and ethylenediamine (90 mg, 1.50 mmol) were dissolved in 20 mL of dry MeOH and stirred for 16 h under N₂ at RT. ¹H NMR analysis of an aliquot taken at this time indicated that the aldehyde was fully consumed. The mixture was then cooled to 0 °C with an ice bath. Sodium borohydride (153 mg, 4.05 mmol) was added to the cooled solution, and the resultant mixture was stirred for 5 h. The MeOH was then stripped from the solution, and the crude product was dissolved in CH₂Cl₂. The crude product was washed with three portions of saturated NaHCO3. Additional product was extracted from the washes with CH₂Cl₂, after which all the organic layers were combined. After the solution was dried over sodium sulfate, the CH2Cl2 was removed to yield the product as a yellow/brown oil (1.10 g, 75% yield). ¹H NMR (400 MHz, CDCl₃, 293 K): δ 6.70 (d, J = 3.2 Hz, 2H), 6.58 (m, 4H), 3.69 (s, 4H), 2.71 (s, 4H), 0.98 (s, 18H), 0.97 (s, 18H), 0.19 (s, 12H), 0.16 (s, 12H). 13 C NMR (100 MHz, CDCl₃, 293 K): δ 149.37, 147.89, 131.51, 121.33, 118.85, 118.5, 49.34, 48.76, 25.84, 25.74, 18.17, 18.15, -4.16, -4.43. MS (ESI): Calcd for MH⁺, 761.4960; Found, 761.4390. IR (cm⁻¹): 2954.75 (m), 2928.86 (m), 2885.76 (w), 2857.11 (m), 1490.24 (s), 1471.75 (m), 1418.47 (w), 1399.57 (w), 1361.42 (w), 1251.29 (s), 1222.56 (s), 1156.34 (w), 1094.93 (w), 982.76 (w), 910.63 (s), 835.60 (s), 799.82 (s), 776.11 (s), 684.52 (m), 666.23 (w), 585.37 (w), 449.33 (w).

N,N'-Bis[2,5-bis(tert-butyldimethylsiloxy)benzyl]-N,N'-bis(tert-butylacetate)-1,2-ethanediamine (3)

N,N'-Bis[2,5-bis(tert-butyldimethylsiloxy)-benzyl]-1,2-ethanediamine (1.10 g, 1.44 mmol), tert-butylbromoacetate (676 mg, 3.47 mmol) and N,N'-diisopropylethylamine (467 mg, 3.61 mmol) were dissolved in 35 mL of CH₂Cl₂ and stirred for 24 h. The solution was diluted with 75 mL of CH₂Cl₂ and washed with three 100 mL portions of saturated NaHCO₃. The organic layer was then washed with brine, dried over Na₂SO₄ for 30 min, and rotavapped to yield a brown oil. The dark brown oil was then dissolved in minimal MeOH. Over the next 16 h, 0.398 g of the product precipitated as a white solid (28% yield). ¹H NMR (400 MHz, CDCl₃, 293 K): δ 6.95 (d, J = 2.8 Hz, 2H), 6.60 (d, J = 8.2, 2H, 6.54 (m, 2H), 3.71 (s, 4H), 3.27 (s, 4H), 2.82 (s, 4H), 1.43 (s, 18H), 0.98 (s, 18H), 0.96 (s, 18H), 0.16 (s, 12H), 0.15 (s, 12H). ¹³C NMR (100 MHz, CDCl₃, 293 K): δ 171.02, 149.54, 147.82, 130.63, 121.06, 118.93, 118.35, 80.42, 55.77, 52.88, 52.78, 28.19, 25.92, 25.77, 18.28, 18.16, -4.13, -4.42. MS (ESI): Calcd for MH⁺, 989.6322; Found, 989.6359. IR (cm⁻¹): 2950.62 (m), 2928.32 (m), 2894.88 (w), 2857.30 (m), 1719.16 (s), 1487.17 (s), 1470.49 (m), 1416.31 (w), 1390.24 (w), 1364.91 (m), 1288.47 (m), 1246.74 (s), 1200.42 (s), 1150.96 (m), 1125.18 (w), 1083.85 (w), 999.09 (w), 973.86 (m), 951.58 (w), 911.60 (s), 888.53 (m), 840.27 (s), 823.08 (s), 693.85 (m), 625.48 (w), 587.08 (m), 542.50 (w), 492.11 (w), 455.49 (w).

N,N'-Bis(2,5-dihydroxybenzyl)-N,N'-bis(tert-butyl-acetate)-1,2-ethanediamine (4)

N,N'-Bis[2,5-bis(tert-butyldimethylsiloxy)benzyl]-N,N'-bis(tert-butylacetate)-1,2-ethanediamine (536 mg, 0.542 mmol) was dissolved in 40 mL of tetrahydrofuran (THF) and cooled to 0 °C. Acetic acid (0.50 mL, 8.7 mmol) and 2.71 mL of a 1.0 M solution of tetra-N-butylammonium fluoride (TBAF) in THF (2.71 mmol) were added. After the reaction mixture stirred for 3 h, 0.60 additional mL of the 1.0 M TBAF solution were added. The resultant solution stirred for another 2 h to ensure full removal of the tert-butyldimethylsilyl groups. 100 mL of water were added to quench the reaction, and the THF was removed by rotavaporation. The product was extracted from the aqueous solution with three 50 mL aliquots of CH₂Cl₂. The combined organic layers were washed with 150 mL of brine before being dried over Na₂SO₄ for 30 min. The crude was purified by column chromatography using 1:1 hexanes/EtOAc as the eluent ($R_f = 0.25$) to yield 222 mg of the product as a yellow oil (77% yield). We were unable to remove impurities that retained either one or two of the silane protecting groups. ¹H NMR (400 MHz, CD₃CN, 293 K): δ 9.06 (bs, 2H), 6.62 (m, 4H), 6.43 (d, J = 2.4, 2H, 6.40 (bs, 2H), 3.61 (s, 4H), 3.15 (s, 4H), 2.62 (s, 4H), 1.45 (s, 18H). 13 C NMR (100 MHz, CD₃CN, 293 K): δ 170.87, 150.24, 149.61, 122.83, 116.40, 116.23, 115.49, 81.41, 56.78, 55.50, 49.29, 27.32. Calcd for MH⁺, 533.2863; Found, 533.2871. IR (cm⁻¹): 3211.89 (w), 2964.06 (m), 1726.78 (s), 1496.02 (s), 1366.96 (s), 1226.52 (s), 1148.54 (s), 983.99 (w), 893.64 (m), 816.58 (m), 776.75 (s), 735.93 (w), 597.05 (w).

N,N'-Bis(2,5-dihydroxybenzyl)ethanediamine-N,N'-diacetic Acid (H₆qc1)

N,*N'*-Bis(2,5-dihydroxybenzyl)-*N*,*N'*-bis(*tert*-butyl-acetate)-1,2-ethanediamine (222 mg, 0.417 mmol) was dissolved in 10 mL of 90:5:5 trifluoroacetic acid/water/triisopropylsilane (TIS) and stirred for 24 h. The solvents were removed by rotavaporation. The product was washed with ether multiple times to remove the residual TIS and dried over air to yield 150 mg of the product as a white powder (86% yield). ¹H NMR (400 MHz, DMSO- d_6 , 293 K): δ 8.83 (s, 2H), 6.62 (m, 6H), 3.93 (s, 4H), 3.60 (s, 4H), 3.14 (s, 4H). ¹³C NMR (100 MHz, DMSO- d_6 , 293 K): δ 170.87, 150.22, 149.20, 120.27, 118.56, 116.94, 116.51, 53.22, 52.84, 50.11. MS (ESI): Calcd for MH⁺, 421.1611; Found, 421.1596. IR (cm⁻¹): 3043.9 (s), 1669.7 (s), 1513.11 (w), 1459.2 (m), 1435.4 (w), 1385.3 (m), 1365.6 (m), 1319.7 (w), 1261 (m), 1193.2 (s), 1131.2 (s), 1010.6 (w), 991.5 (w), 968.3 (w), 907.4 (w), 840.6 (m), 799.9 (m), 760.1 (m), 719.1 (m). UV/vis (50 HEPES buffered to pH 7.4): 294 nm (3500 M⁻¹ cm⁻¹).

3. Results

3.1. Synthesis of H₆qc1

The ligand can be prepared in five steps from commercially available starting materials (Scheme 3); the first intermediate, 2,5-bis(tertbutyldimethylsiloxy)benzaldehyde (1), was previously synthesized by another research group [20]. The synthesis of H₆qc1 is more difficult than those used to prepare H₄qp2 and the related H₂qp1 (Scheme 2) for several reasons. First, two additional steps are required due to the need to protect both the quinols and the carboxylic acids. With H₂qp1 and H₄qp2, conversely, the quinols are added to the ligand framework late enough in the synthesis to obliviate the need for their protection [7,8]. Second, two of the intermediates need to be purified by column chromatography. H₂qp1 can be obtained in high purity without any chromatography [7]; whereas, H₄qp2 requires just a single column at the end of the synthesis [8]. Third, the addition of the protected carboxylic acids to yield 3 proved to be challenging. We eventually found that highly pure material would precipitate from MeOH, albeit in low yield (28%). Alternative means of purifying 3, including column chromatography, did not effectively remove impurities. The immediate precursor to H₆qc1, 4, could not be obtained in high purity, but the impurities

Scheme 3. Synthesis of H₆qc1.

were removed in the final step of the synthesis, as confirmed by NMR.

We attempted to isolate a Mn(II) complex with H₆qc1 but were unable to precipitate clean material from a variety of solvents, including water, MeCN, CH2Cl2, and MeOH. Given this, studies on the Mn (II) were done on samples prepared in situ; this has been done with other manganese-containing complexes, including some MRI contrast agents [11-13].

3.2. Aqueous characterization of the H_6qc1 ligand

We analyzed the behavior of the H₆qc1 ligand by itself in an aqueous solution containing 100 mM KCl via potentiometric pH titrations. Our best fitting model for the titration data displays five ionization events as the pH increased from 2 to 10.5 (Table 1, Fig. S19). We did not collect or model data past pH 10.5, as was done with HBED [13,14], since the ligand displays irreversible degradation under those conditions. Using the speciation of HBED as a model, the H₆qc1 ligand likely exists as [H₈qc1]²⁺ under extremely acidic conditions, with the extra

Table 1 pMn and pKa values for the ligands and Mn(II) complexes with H₆qc1 determined by potentiometric titration at 25 °C.

pK_{L1}^{a}	$11.7 (\pm 0.3)$	pK _{a1} ^b	$8.02 (\pm 0.06)$
pK_{L2}^{a}	$8.80 (\pm 0.05)$	pK_{a2}^{b}	$6.19 (\pm 0.06)$
pK_{L3}^{a}	$4.31 (\pm 0.05)$	pK_{a3}^{b}	$4.24 (\pm 0.06)$
pK_{L4}^{a}	$2.89 (\pm 0.05)$	log K(MnH ₃ qc1) ^c	15.59
pK _{L5} ^a	$2.45 (\pm 0.3)$	log K(MnH₄qc1) ^c	10.11
		log K(MnH ₅ qc1) ^c	5.55
		pMn (pH 7.4) ^d	6.67

^a Ligand pK_a values correspond to the following equilibrium constants: $K_{L1} = [(H_3qc1)^-][H^+]/[(H_4qc1)^2-], pK_{L1} = log\beta_{110} - log\beta_{010}; K_{L2} = [(H_4qc1)^2-]$ $[H^+]/[(H_5qc1)^-], pK_{L2} = log\beta_{210} - log\beta_{110}; K_{L3} = [(H_5qc1)^-][H^+]/[(H_6qc1)],$ $pK_{L3} = log\beta_{310} - log\beta_{210}; \quad K_{L4} = [(H_6qc1)][H^+]/[(H_7qc1)^+], \quad pK_{L4} = log\beta_{410} - log\beta_{410} - log\beta_{410}]$ $\log \beta_{310}$; $K_{L5} = [(H_7qc1)^+][H^+]/[(H_8qc1)^{2+}]$, $pK_{L5} = \log \beta_{510} - \log \beta_{410}$.

two protons localized on each of the amines [14]. The first three ionization events correspond to p K_a values of 2.45 (\pm 0.3), 2.89 (\pm 0.05), and 4.31 (\pm 0.05). These likely correspond to the deprotonation of the first ammonium and the two carboxylic acids and the formation of H_7qc1^+ , H_6qc1 , and H_5qc1^- . The amine and the carboxylate conjugate bases are anticipated to accept intramolecular hydrogen bonds from the remaining ammonium and the two quinols, as was seen in the crystal structure of the free H_2qp1 ligand [21]. The other two pK_a values resulting from the model are 8.80 (\pm 0.05) and 11.7 (\pm 0.3); the associated deprotonation reactions yield H_4qc1^{2-} and H_3qc1^{3-} . The error in the 11.7 p K_a is larger since we could not fully generate the species during the titrations. The related HBED ligand displays similar acid/ base chemistry, with p K_a values of 1.7, 2.53, 4.72, 8.44, and 11.00, plus another at 12.60 [14]. The UV/vis spectrum of H₆qc1 in water changes substantially as the pH increases from 7.4 to 9.0 (Fig. S21). At low pH values, there is a strong feature at 299 nm, which is consistent with a phenol or quinol group [8,10]. As the solution becomes more basic, however, a lower-energy band at 330 nm develops; the energy of this feature is more consistent with a phenolate or quinolate group. The proton that is lost from the ligand as the pH increases from 7.4 to 9.0 appears to be at least partially localized on the quinol. Between pH 7.0 and 7.4, the H₆qc1 ligand therefore predominantly exists as H₅qc1⁻, with a trace amount of H_4qc1^{2-} (Fig. 1).

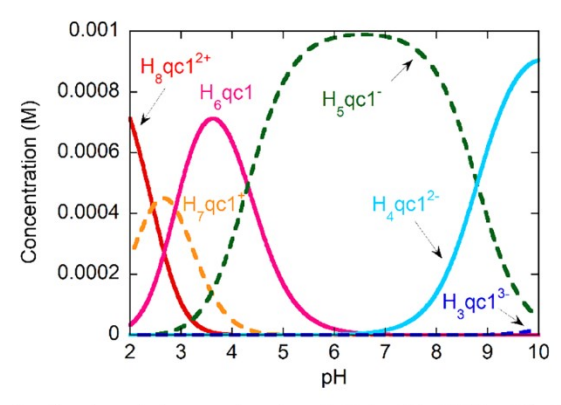


Fig. 1. Predicted speciation as a function of pH for 1.0 mM H₆qc1 in 100 mM KCl solution.

Metal complex pK_a values correspond to the following equilibrium constants: $K_{a1} = [[Mn(H_2qc1)]^2 -][H^+]/[[Mn(H_3qc1)]^-], pK_{a1} = log\beta_{011} - log\beta_{011}$ $_{111}; K_{a2} = [[Mn(H_3qc1)]^-][H^+]/[[Mn(H_4qc1)]], pK_{a12} = log\beta_{111} - log\beta_{011}.;$ $K_{a3} = \hbox{\tt [[Mn(H_4qc1)]][H^+]/[[Mn(H_5qc1)^+]], pK$_{a13}$ = $\log\beta_{211} - \log\beta_{111}$.}$

^c Metal complex stability constants correspond to the following equilibrium constants: $K(MnH_3qc1) = [[Mn(H_3qc1)^-]]/[Mn^{2+}][H_3qc1^{3-}]; K(MnH_4qc1) =$ $[[Mn(H_4qc1)]]/[Mn^{2+}][H_4qc1^{2-}]; \quad K(MnH_5qc1) = [[Mn(H_5qc1)^+]]/[Mn^{2+}][H_5-R_5]$ qc1 $\bar{}$]. d log(free Mn(II)) at pH 7.4 with 1.0 mM Mn(II) and 1.0 mM $H_6qc1.$

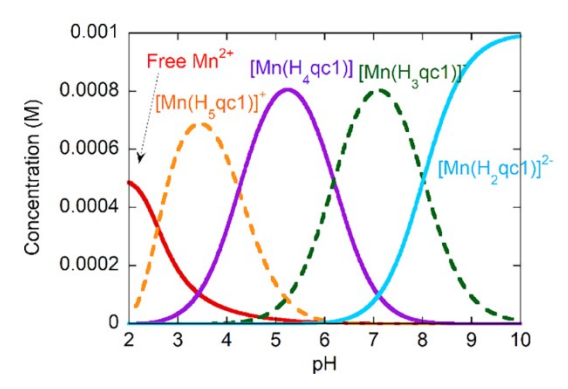


Fig. 2. Predicted speciation of Mn(II) as a function of pH for an aqueous solution containing $1.0\ mM\ MnCl_2,\, 1.0\ mM\ H_6qc1$, and $100\ mM\ KCl.$

3.3. Aqueous characterization of the Mn(II) complex with H_6qc1

The speciation of Mn(II) complexes with H₆qc1 in water was analyzed using a 100 mM solution of KCl containing a 1:1 mixture of MnCl₂ and ligand. The curves resulting from the potentiometric pH titrations (Fig. S22) look distinct from those for the metal-free H₆qc1, and only four clear ionization events are observed as the pH is increased from 2.6 to 10.2. As with our analysis of the titration data for free H₆qc1, the inclusion of additional species into the model worsened the fit (Fig. S23). The lowest pH ionization event corresponds to the release of Mn (II) from the ligand. The next three ionization events are assigned to (de)protonation events for the H₆qc1-Mn(II) complex and correspond to pK_a values of 4.24 (\pm 0.06), 6.19 (\pm 0.06), and 8.02 (\pm 0.06) (Table 1). The UV/vis bands of an aqueous 1:1 mixture of MnCl2 and H₆qc1 change substantially from pH 5 to 9 (Fig. S24), leading us to assign the 6.19 and 8.02 p K_a values to the deprotonation of the Mn(II)bound quinols [8]. The acid/base behavior is similar to that of the Mn (II) complex with HBED, which has pK_a values of 6.58 and 7.66 for the deprotonation of Mn(II)-bound phenols [13].

The speciation of the Mn(II) as a function of pH is shown in Fig. 2. Our model of the data suggests that the Mn(II)- H_6 qc1 complex is indeed more stable than Mn(II)- H_4 qp2 but is less stable than Mn(II)- H_2 qp1 The pMn value at pH 7.4, 1.0 mM total Mn(II), and 1.0 mM total ligand is 6.67; the pMn values for the H_2 qp1 and H_4 qp2 systems under identical conditions, conversely, were found to be 7.25 and 5.36, respectively [8,22]. At pH 7, the Mn(II) exists predominantly as [Mn(H_3 qc1)]⁻, with a substantial amount of [Mn(H_2 qc1)]². Since we could not assess the stability of the fully deprotonated ligand, H_2 qc1⁴-, we were unable to measure a K_{eq} value for the complexation of the tetraanionic ligand with Mn(II), but we were able to measure values for the Mn(II) complexes with H_5 qc1⁻, H_4 qc1²-, and H_3 qc1³- (Table 1). The Mn(II) complexes with doubly and triply deprotonated HBED appear to be less stable than their H_6 qc1 analogs, with log K values of 5.56 and 9.98 respectively [13].

3.4. Oxidative stability of the H_6qc1 ligand and its Mn(II) complex

Neither the ligand nor its Mn(II) complex appears to react with O_2 in aqueous solution over several hours as assessed by UV/vis analysis of solutions of these compounds exposed to air (Figs. S25 and S26). The UV/vis spectrum of each compound remains approximately the same. The stability of the Mn(II) complex to air was also confirmed by EPR (Fig. S27). Although the H_6 qc1 ligand by itself does not react with H_2O_2 over the course of 1 h (Fig. S28), its Mn(II) complex reacts quickly with this oxidant as assessed by both UV/vis and EPR. In 50 mM HEPES buffered to pH 7.0, the Mn(II) complex initially displays three bands at 298 nm, 368 nm, and 481 nm (Fig. 3). Upon the addition of H_2O_2 , all three peaks increase in intensity over the course of 5 min but then weaken. The band at 298 nm eventually disappears completely,

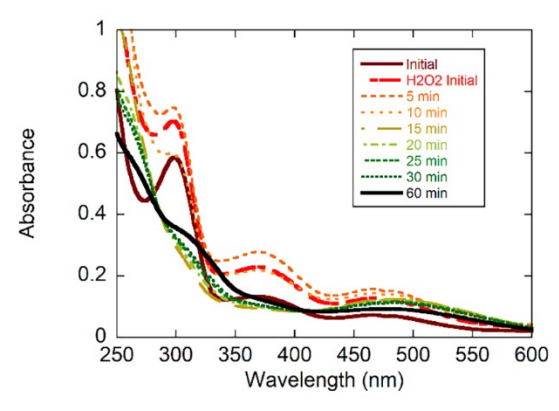


Fig. 3. Spectrophotometric response of an aqueous solution containing 0.1 mM MnCl₂, 0.1 mM H₆qc1, and 50 mM HEPES buffered to pH 7.0 to 43 mM H₂O₂.

suggesting that the quinols have been oxidized. Over the course of 1 h, a broad band centered at 482 nm steadily develops. UV/vis peaks with similar energies have been previously observed for Mn(III) species [23,24]. Parallel reactions analyzed by EPR confirm that the metal is being oxidized to an EPR-silent species, with the Mn(II) signal steadily vanishing over 30 min (Fig. 4). We are currently unable to separate these oxidized manganese products and have therefore been unable to obtain stability measurements for any of the individual species.

We were unable to obtain clean samples of the demetallated and oxidized form(s) of the ligand. We instead analyzed the ligand oxidation by adding $\rm Zn(OTf)_2$ to reactions containing 1:1 mixtures of $\rm H_6qc1$ and $\rm MnCl_2$ with or without $\rm H_2O_2$. The $\rm Zn(II)$ displaces the manganese from the ligand, yielding species that can be readily visualized by $\rm ^1H$ NMR. The addition of $\rm H_2O_2$ decreases the intensity of the aromatic peaks relative to the benzylic ones; this is consistent with the loss of the OH protons and the oxidation of the quinols to $\it para$ -quinones (Fig. S29) [7,8].

3.5. Measurement of T_1 -weighted relaxivity for Mn(II)-H₆qc1 and its oxidized products

The Mn(II) complex with H_6qc1 displays distinct spectroscopic changes upon reaction with H_2O_2 , but not O_2 , prompting us to investigate whether the compound could selectively detect H_2O_2 via

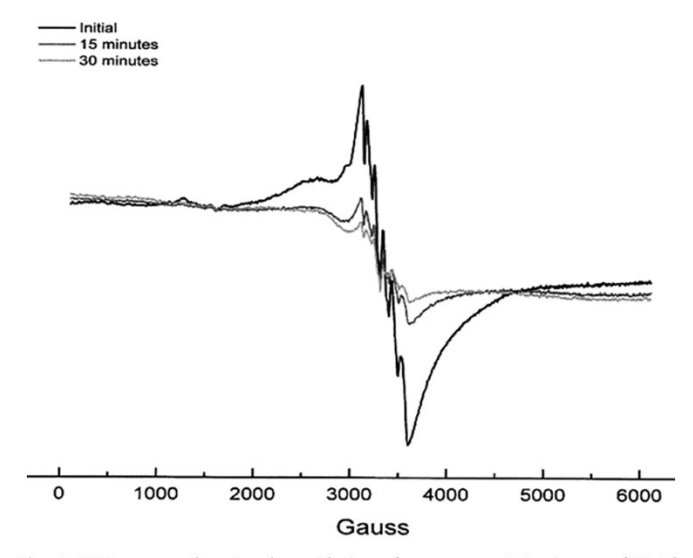


Fig. 4. EPR spectra showing the oxidation of an aqueous 1:1 mixture of $MnCl_2$ and H_6qc1 by H_2O_2 over 30 min. All solutions contained 1.0 mM $MnCl_2$, 1.0 mM H_6qc1 , and 50 mM HEPES buffered to pH 7.0. 10 mM of H_2O_2 was added, and the reaction was allowed to proceed at RT. Aliquots were removed and frozen for EPR analysis at 15 min and 30 min.

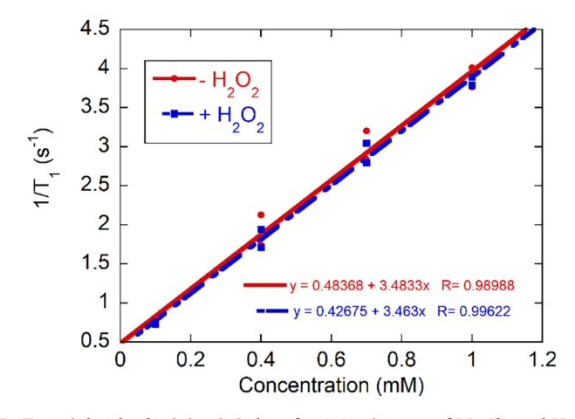


Fig. 5. T_1 -weighted relaxivity (r_1) data for 1:1 mixtures of MnCl₂ and H₆qc1 in the absence and presence of excess (10 mM) H₂O₂ in an aqueous solution containing 50 mM Na₃PO₄ buffered to pH 7.00. All samples were analyzed at 298 K with a 3 T clinical MRI scanner. All samples were prepared under air and run within 30 min of preparation.

changes in its T_1 -weighted relaxivity (r_1) . We characterized the reaction between H₂O₂ and the Mn(II)-H₆qc1 complex using methodology that we had developed for prior H_2O_2 sensors [6-8]. We measured the T_1 values of 1:1 mixtures of MnCl2 and H6qc1 in aqueous solutions buffered to pH 7.0 using a 3T MRI scanner. The concentration of Mn(II) was varied from $0.10 \,\mathrm{mM}$ to $1.0 \,\mathrm{mM}$, and the slope of $(1/T_1)$ versus the concentration provides r_1 . A second set of solutions contained 10 mM H₂O₂ in order to oxidize the Mn(II)-H₆qc1 complex; these were allowed to react for 30 min in order to ensure that the reactions went to completion. Unexpectedly, the presence of H₂O₂ neither increased nor decreased the r_1 of the manganese/H₆qc1 mixtures. In phosphate buffer, the r_1 values before and after adding H_2O_2 , 3.48 and 3.46 mM⁻¹ s⁻¹, are within error of each other (Fig. 5). A significant response to H₂O₂ was likewise absent when the complex was studied in 50 mM HEPES buffered to pH 7.0. In one instance, we observed a 10% increase in r_1 (Fig. S30), but this was not reproducible.

4. Discussion

Redox-active ligands have found increasing use within many subfields of inorganic chemistry [25–31]. Our own interest in this area has centered on using quinol-containing molecules to prepare complexes that display oxidation-triggered increases in their T_I -weighted relaxivity (r_I) and/or catalyze the degradation of superoxide [7,8,21]. Both applications rely upon the quinols within the organic ligands reversibly oxidizing to para-quinones (Scheme 1). The first two polydentate ligands, H_2 qp1 and H_4 qp2 (Scheme 2), use amines and pyridines as the other chelating groups. Although their complexes with Z_I (II) thus far appear to be highly stable in water [21], these neutral N-donors bind much more weakly to Z_I (II) [8]. As a consequence, the Z_I (II) and its oxidation to complexes with the di- Z_I (II) and its oxidation to complexes with the di- Z_I (II) and mono- Z_I (II) and mono- Z_I (III) and mono- Z_I (III) are complexes with the di- Z_I (III) and mono- Z_I (III) are complexes with the di- Z_I (III) and mono- Z_I (III) are complexes with the di- Z_I (III) and mono- Z_I (III) are complexes with the di- Z_I (III) and mono- Z_I (III) are complexes with the di- Z_I (III) and mono- Z_I (III) are complexes with the di- Z_I (III) and mono- Z_I (III) are complexes with the di- Z_I (III) and mono- Z_I (III) are complexes with the di- Z_I (III) and mono- Z_I (III) are complexes with the di- Z_I (III) and mono- Z_I (III) are complexes with the di- Z_I (III) and mono- Z_I (III) are complexes with the di- Z_I (III) and mono- Z_I (III) are complexes with the di- Z_I (III) and mono- Z_I (III) are complexes with the di- Z_I (III) and mono- Z_I (III) are complexes with the di- Z_I

In order to prepare a ligand that can more tightly coordinate Mn(II), we have replaced the pyridines of H_4qp2 with carboxylic acids to yield H_6qc1 (Scheme 2). Although the ligand is much more challenging to synthesize than H_4qp2 , the changes to the molecule do improve its affinity for Mn(II). The pMn value for H_6qc1 (pH 7.4, 1.0 mM total Mn (II), 1.0 mM total ligand) is 6.67, which is over an order of magnitude improvement over the 5.36 value reported for the H_4qp2 system but is worse than the 7.25 value measured for H_2qp1 [8,22]. Substantial metal dissociation is still observed under highly acidic conditions (Fig. 2). The superior binding affinity of H_2qp1 for Mn(II) is initially difficult to rationalize, since the latter ligand cannot attain as negative a charge. The quinol portions of the ligands, however, appear to bind to

Scheme 4. Structure of Hptp1 ligand.

metal ions poorly in their neutral forms, and they are often detached from the metal ions in crystal structures [8,21]. Under neutral to acidic conditions, $\rm H_2qp1$ consistently provides five strong donor atoms as opposed to the four from $\rm H_6qc1$. We believe that the extra effective donor atom of $\rm H_2qp1$ more than compensates for its less negative charge, particularly under acidic conditions.

Unexpectedly, the quinols appear to bind to the Mn(II) much more tightly than phenols. The stability constants of the [Mn(H₃qc1)] $^-$ and [Mn(H₄qc1)] complexes (Table 1) are higher than those for their analogs with the related HBED ligand, which contains phenols instead of the quinols found in H₆qc1 (Scheme 2) [13]. This appears to be a reproducible effect since the Mn(II) complex with H₂qp1 is substantially more stable than the Mn(II) complex with Hptp1 (Scheme 4), which has a pMn of 5.40 at pH 7.4 [15]. The OH group para to the coordinating Odonor of the quinol is a more strongly electron-donating substituent than the H group that occupies its place in a phenol. We speculate that the OH for H substitution renders quinolates more electron-rich and thereby increases their affinities for metal ions.

The more anionic charge of the H_6qc1 ligand has a weak impact on the interaction between the quinols and the metal center. The Mn(II) complexes with H_6qc1 and H_4qp2 have similar pK_a values for their Mn (II)-quinol groups: 6.19 and 8.02 for H_6qc1 versus 5.82 and 7.14 for H_4qp2 [8]. The acid/base behavior of the Mn(II) complex with H_6qc1 strongly resembles that observed for its analog with HBED, which has pK_a values of 6.58 and 7.66 [13].

Highly anionic ligands, such as ethylenediaminetetraacetate (EDTA⁴⁻), often stabilize Mn(III) species [32], and the more negatively charged coordination sphere provided by H₆qc1 around pH 7 does render the metal center more susceptible to oxidation. Neither the H₄qp2 nor the H₆qc1 complex with Mn(II) displays any substantial spectroscopic change upon a 4h reaction with air. [Mn(H4qp2)Br2] is slowly oxidized to a Mn(III) species upon reaction with H₂O₂, but this is not noticeable by EPR at $30 \, \text{min}$ [8]. The Mn(II) complex with H₆qc1, conversely, quickly reacts with H₂O₂ to yield what we believe are one or more Mn(III)-containing products, as assessed by both UV/vis and EPR (Figs. 3 and 4). Oxidation to Mn(IV) is unlikely. This oxidation state is readily observable by EPR, but new signals do not appear in the EPR spectrum of the H₆qc1 complex as the reaction with H₂O₂ proceeds. The ligand appears to be oxidized as well, as evidenced by both UV/vis and ¹H NMR (Figs. 3 and S29). We have thus far been unable to isolate any individual manganese-containing products from these reaction mixtures.

It is challenging to predict the overall impact of H_2O_2 on the T_I -weighted relaxivity of the manganese complex with H_6qc1 since both the ligand and metal are being oxidized during the reaction. The Mn(II) sensors with H_2qp1 and H_4qp2 react with H_2O_2 to yield Mn(II) species with higher r_I values, which we attributed to water molecules displacing the para-quinone groups of the oxidized ligands (Scheme 1) [7,8]. More highly aquated metal centers tend to have higher r_I values. The oxidation of the Mn(II) by H_2O_2 , conversely, would be anticipated to

worsen the r_1 since the metal ion is rendered less paramagnetic by this process [10,33]. Another factor that impacts r_1 is the rate of water exchange. Oxidation to Mn(III) would be anticipated to slow the rate of exchange [34], but the value that would optimize r_1 has not yet been established for either Mn(II) or Mn(III) complexes. Unexpectedly, the oxidation of 1:1 Mn(II)/H₆qc1 mixtures by H₂O₂ results in no observable change to the r_1 at pH 7.0 (Fig. 5). The relaxivity is impacted by the choice of buffer; the Mn(II)- H_6qc1 complex is more effective in 50 mM HEPES solution $(3.98 \text{ mM}^{-1} \text{ s}^{-1})$ than in 50 mM phosphate $(3.48 \,\mathrm{mM}^{-1}\,\mathrm{s}^{-1})$. Phosphate is known to compete with superoxide in manganese-containing superoxide dismutase mimics [15,35,36], and this may decrease r_1 by competing with water for vacant coordination sites on the metal ion. In one set of experiments, we observed a 10% increase in r_1 in HEPES solution upon adding H_2O_2 (Fig. S30), which is much smaller than the 30% increase we observed for the H₄qp2 system [8], but we could not replicate this in other experiments. Determining whether the metal center is indeed become more highly aquated during the reaction with H₂O₂ is complicated by the lack of a protocol for measuring solution state aquation numbers for Mn(III) species.

5. Conclusion

The substitution of two carboxylate groups for the pyridines in the H_4 qp2 ligand allows the resultant H_6 qc1 ligand to bind more tightly to Mn(II). Unfortunately, the more anionic coordination sphere facilitates oxidation of the metal center, which in turn, eliminates the H_2O_2 -triggered increase in T_1 -weighted relaxivity that was observed for the related H_4 qp2 probe. Although the new ligand is unsuitable for manganese-containing MRI contrast agent sensors for H_2O_2 , the presence of redox-active functionalities and its strongly anionic charge may make this ligand useful for other applications.

Acknowledgements

This work was supported by Auburn University and a grant from the National Science Foundation (NSF-CHE-1662875). We thank Prof. Evert Duin for his assistance with acquiring the EPR data and Mr. Owen Chandler for helpful discussions regarding the synthesis of the ligand.

Appendix A. Supplementary data

Supplementary data to this article can be found online at https://doi.org/10.1016/j.ica.2019.119045.

References

[1] L. Tretter, I. Sipos, V. Adam-Vizi, Neurochem. Res. 29 (2004) 569-577.

- [2] C.K. Roberts, K.K. Sindhu, Life Sci. 84 (2009) 705-712.
- [3] R.L. Mosley, E.J. Benner, I. Kadiu, M. Thomas, M.D. Boska, K. Hasan, C. Laurie, H.E. Gendelman, Clin. Neurosci. Res. 6 (2006) 261–281.
- [4] I.M. Fearon, S.P. Faux, J. Mol. Cell. Cardiol. 47 (2009) 372-381.
- [5] G. Eskici, P.H. Axelsen, Biochemistry 51 (2012) 6289-6311.
- [6] M. Yu, R.J. Beyers, J.D. Gorden, J.N. Cross, C.R. Goldsmith, Inorg. Chem. 51 (2012) 9153–9155.
- [7] M. Yu, S.L. Ambrose, Z.L. Whaley, S. Fan, J.D. Gorden, R.J. Beyers, D.D. Schwartz, C.R. Goldsmith, J. Am. Chem. Soc. 136 (2014) 12836–12839.
- [8] M. Yu, M.B. Ward, A. Franke, S.L. Ambrose, Z.L. Whaley, T.M. Bradford, J.D. Gorden, R.J. Beyers, R.C. Cattley, I. Ivanović-Burmazović, D.D. Schwartz, C.R. Goldsmith, Inorg. Chem. 56 (2017) 2812–2826.
- [9] S.L. O'Neal, W. Zheng, Curr. Environ. Health Rep. 2 (2015) 315-328.
- [10] E.M. Gale, S. Mukherjee, C. Liu, G.S. Loving, P. Caravan, Inorg. Chem. 53 (2014) 10748–10761.
- [11] E.M. Gale, I.P. Atanasova, F. Blasi, I. Ay, P. Caravan, J. Am. Chem. Soc. 137 (2015) 15548–15557.
- [12] G.S. Loving, S. Mukherjee, P. Caravan, J. Am. Chem. Soc. 135 (2013) 4620-4623.
- [13] F. L'Eplattenier, I. Murase, A.E. Martell, J. Am. Chem. Soc. 89 (1967) 837-843.
- [14] R.J. Motekaitis, A.E. Martell, M.J. Welch, Inorg. Chem. 29 (1990) 1463-1467.
- [15] I. Kenkel, A. Franke, M. Dürr, A. Zahl, C. Dücker-Benfer, J. Langer, M.R. Filipović, M. Yu, R. Puchta, S.R. Fiedler, M.P. Shores, C.R. Goldsmith, I. Ivanović-Burmazović, J. Am. Chem. Soc. 139 (2017) 1472–1484.
- [16] Q. Zhang, J.D. Gorden, R.J. Beyers, C.R. Goldsmith, Inorg. Chem. 50 (2011) 9365–9373.
- [17] M.A. Bernstein, K.F. King, X.J. Zhou, Handbook of MRI Pulse Sequences, Elsevier Academic Press, Amsterdam, 2004.
- [18] E.M. Haacke, R.W. Brown, M.R. Thompson, R. Venkatesan, Magnetic Resonance Imaging: Physical Principles and Sequence Design, John Wiley & Sons, New York, NY. 1999.
- [19] J.A. Nelder, R. Mead, Comput. J. 7 (1965) 308-313.
- [20] J. Yoon, J.-S. Ryu, Bioorg. Med. Chem. Lett. 20 (2010) 3930-3935.
- [21] M.B. Ward, A. Scheitler, M. Yu, L. Senft, A.S. Zillmann, J.D. Gorden, D.D. Schwartz, I. Ivanović-Burmazović, C.R. Goldsmith, Nat. Chem. 10 (2018) 1207–1212.
- [22] A. Franke, A. Scheitler, J.L. Moore, S. Sader, S. Ison, I. Ivanović-Burmazović, C.R. Goldsmith, unpublished results.
- [23] C.R. Goldsmith, A.P. Cole, T.D.P. Stack, J. Am. Chem. Soc. 127 (2005) 9904–9912.
- [24] T.J. Hubin, J.M. McCormick, N.W. Alcock, D.H. Busch, Inorg. Chem. 40 (2001) 435–444.
- [25] J.T. Henthorn, S. Lin, T. Agapie, J. Am. Chem. Soc. 137 (2015) 1458-1464.
- [26] I.R. Corn, P.D. Astudillo-Sánchez, M.J. Zdilla, P.E. Fanwick, M.J. Shaw, J.T. Miller, D.H. Evans, M.M. Abu-Omar, Inorg. Chem. 52 (2013) 5457–5463.
- [27] M.R. Haneline, A.F. Heyduk, J. Am. Chem. Soc. 128 (2006) 8410–8411.
- [28] T. Hirao, Coord. Chem. Rev. 226 (2002) 81-91.
- [29] T.W. Myers, L.A. Berben, Inorg. Chem. 51 (2012) 1480–1488.
- [30] D.L.J. Broere, R. Plessius, J.I. van der Vlugt, Chem. Soc. Rev. 44 (2015) 6886-6915.
- [31] O.R. Luca, R.H. Crabtree, Chem. Soc. Rev. 42 (2013) 1440-1459.
- [32] F.A. Cotton, G. Wilkinson, Advanced Inorganic Chemistry, fifth ed., John Wiley & Sons, New York, 1988.
- [33] P. Caravan, J.J. Ellison, T.J. McMurry, R.B. Lauffer, Chem. Rev. 99 (1999) 2293–2352.
- [34] A. Cusanelli, U. Frey, D.T. Richens, A.E. Merbach, J. Am. Chem. Soc. 118 (1996) 5265–5271.
- [35] D. Lieb, F.C. Friedel, M. Yawer, A. Zahl, M.M. Khusniyarov, F.W. Heinemann, I. Ivanović-Burmazović, Inorg. Chem. 52 (2013) 222–236.
- [36] F.C. Friedel, D. Lieb, I. Ivanović-Burmazović, J. Inorg. Biochem. 109 (2012) 26–32.